Reply to report of reviewer #1
"Errors in satellite-based global horizontal irradiance retrievals due to three-dimensional cloud-radiation interactions by Wiltink et. al."

bold italic font = reviewer's comment
regular font = authors' reply
red regular font = original text in the manuscript
blue regular font = newly added or updated text in the manuscript

---

General comments

This study evaluates errors in satellite retrievals of global horizontal irradiance (GHI) due to three-dimensional (3D) cloud-radiation interactions at different spatial resolutions (from fine (50 m) to coarse resolutions (12.4 km)). This is achieved by utilizing two shallow-cumulus Large Eddy Simulations (LES) cloud fields, alongside retrieval algorithms and both 3D and 1D radiative transfer framework to perform a comprehensive study via a 1D/3D GHI retrieval vs 1D/3D GHI reference pathway approach, and mapping of differences to plane parallel approximation (PPA), independent pixel approximation (IPA) and residual biases. They show that at fine spatial resolutions current retrieval algorithms assuming the IPA prove to be insufficient to accurately resolve heterogeneous cloud conditions and emphasize the need to develop 3D RT parameterizations and corrections for GHI retrievals.

The work is well motivated, interesting, and the manuscript is mostly well written. There are a few areas where I think more examples and explanations are needed. For example, the study was mostly based on nadir viewing ($\theta = 0^\circ$) to avoid parallax error, even though geostationary satellites viewing zenith observations over mid-latitudes are typically off-nadir. The study also includes slant-view case ($\theta = 70^\circ$) and discusses parallax induced smoothing, but the operational message ("The current generation of geostationary satellites already resolves these finer spatial scales in which IPA-related errors dominates") partly depends on typical viewing conditions. It would be interesting to add one intermediate viewing zenith angle (e.g., 35 - 45°) to bridge between overhead (0°) and extreme (70°) view zenith. Also, since this study is based on two cloud fields of the same cloud type (shallow cumulus clouds), care should be taken to draw conclusions objectively from the results. These are all minor concerns and are stated in my specific comments below. I congratulate the authors for this great work and, after addressing these remarks, I recommend prompt publication in ACP.

We thank the reviewer for taking the time to review our document and provide constructive feedback. We agree that caution is required when generalising, for instance, to other cloud types. This study focuses on two highly variable cumulus cloud fields; hence, 3D cloud-radiation interactions are likely to be less prominent under more homogeneous conditions. However, since this has not been investigated in the current study, it should be mentioned more clearly. We will clarify this in the Conclusions and Outlook section:

P29 L555: Two highly variable [...] are studied. Since this study only presents results for two highly variable cumulus cloud fields, future studies should clarify how the presented results generalise to other cloud conditions.

Moreover, since reviewer #2 also expressed concern about remaining uncertainties and generalisability, we have decided to include an additional discussion section addressing these topics. For further details, please see our reply

to reviewer #2.

Finally, please find our response to the point raised about intermediate viewing angles in the corresponding specific comment below.

Specific comments

L97: Do both cloud scenarios have the same cloud top height (CTH) of 6.4 km? If not, state the CTH of each cloud scene and briefly explain how the CTH and cloud base height (CBH) of the two cloud fields were obtained.
The 6.4 km mentioned in the article refers to the domain top height in the LES simulations and does not represent the cloud top height. The actual cloud top (and bottom) heights are variable depending on the liquid water content of the grid cells from the LES output. To indicate cloud height, we will mention the domain-averaged cloud-top and cloud-bottom heights (excluding clear-sky pixels) for both scenes in the revised manuscript. The cloud top and bottom heights are derived for each column as the highest/lowest level where LWC > 0 kg m^{-3}, respectively.

Page 4, L103: The cloud cover [..] is 22%. The cloud base and cloud top heights, as determined from the lowest and highest level with a non-zero liquid water content, vary over the domain. The domain-averaged cloud base and top heights are 1550 m and 1867 m, respectively.
Page 4, L105 Compared to [..] 64 %. Compared to scene 1, the domain-averaged cloud base and cloud top are slightly higher, at 1884 m and 2126 m, respectively.

L113: Reference this study: https:/doi.org/10.1029/2022JD036822 and include it in the discussion. Ambient aerosols have been shown to have a significant impact on the 3D radiative effect of cumulus scenes such as those considered in this work.
We thank the reviewer for bringing this publication to our attention. We will include the reference in the new Section discussing generalisability and remaining uncertainties. See reply to reviewer #2.

L118-119: Provide a justification for rounding the scene cloud droplet effective radii to their nearest integer values. The authors referred to Sect 3.1 where we see the range of droplet radii for MONKI simulations as 3 to 22 µm in 1 µm steps, but no satisfactory justification was made.
The rounding of cloud droplet effective radii was done for practical considerations related to the simulation of synthetic TOA reflectances. To run the MONKI Monte Carlo code, for each droplet size, files containing information on scattering properties are required (e.g., scattering phase functions). These files were generated with the Meerhof Mie Program. As long as the scattering files are available, MONKI can also simulate reflectances for intermediate effective cloud droplet radii. However, including a wider range of droplet sizes in a single simulation reduces computational performance. Since the simulations were already computationally intensive, we have decided not to further increase the number of cloud droplet effective radii.

We will add a justification to the document:
Page 6, Line 145: The range [..] is 3 to 22 µm in steps of 1 µm. This step size was used since including droplet sizes with smaller steps would make the MONKI simulations computationally unfeasible.

Fig. 1: I really like this figure. It captures the descriptions of the methods in the text. Two comments:

1. ***The rectangle in the topmost row showing the reflectance output from MONKI (3D), it will be helpful to include "(3D)" to the VIS/NIR reflectances. This would aid swift visualization that the reflectances here are from 3D RT and readers can grab the big picture by just looking at the figure.***
2. ***Try to indicate that the CPP-SICCS in the first two rows are based on plane-parallel atmosphere and the different columns are independent. Like include "(1D RT theory)" or "1D"***

We thank the reviewer for these suggestions. The figure has been updated based on the above-mentioned comments.

L164-167: cloud mask is generated based on the liquid water path from the LES data based on LES LWP > 0, while retrieved optical depth can return small non-zero τ even in clear pixels, and a separate τ> 0 condition is also mentioned for cloudy masking. Because much of the mechanism relies on pixels being (mis)classified as cloudy/clear (especially enhancement/shading), inconsistencies here could affect residual attribution. What is the mismatch frequency between (LWP> 0) and (retrieved τ > 0) at each resolution (or at least at 50 m and one coarser scale)? Show that the main conclusions are not driven by classification artifacts. Consider reporting a sensitivity where the retrieval uses the retrieved τ threshold consistently for SICCS cloudy/clear (even if only for one scenario).

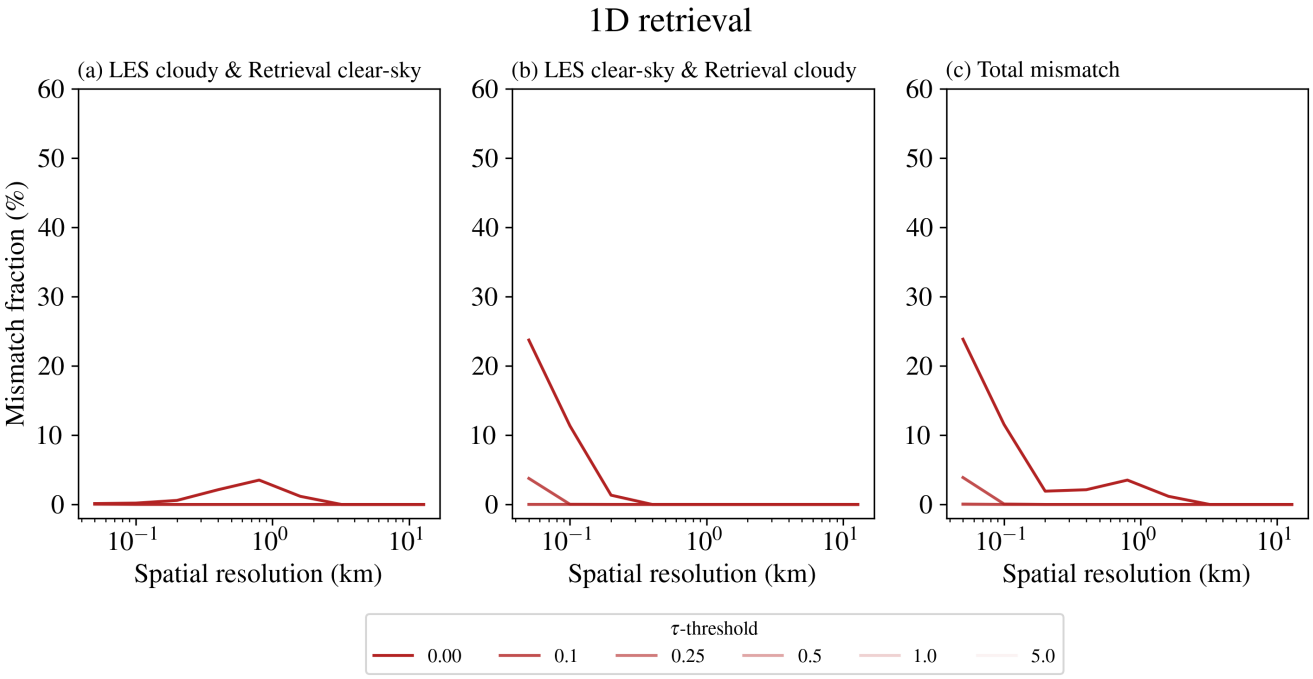

Figure R1.1: Mismatch fractions between cloud masks for the 1D retrieval: (a) LES cloudy and retrieved clear-sky; (b) LES clear-sky and retrieved cloudy; (c) total mismatch error. Results are shown for the default scenario, where apart from the standard $\tau = 0$ threshold to separate clear and cloudy pixels also other τ thresholds are included.

Two cloud masks are indeed used in this study, and they are not identical. The LES cloud mask is used throughout the paper, but the retrieval has its own cloud mask based on the inferred cloud optical thickness. We have performed an analysis of the mismatch between these cloud masks for the 1D and 3D retrieval. The sensitivity to hypothetical τ-thresholds larger than zero is also analysed.

1D retrieval

The misclassification for the 1D retrieval remains limited. The mismatch fraction for pixels being cloudy in the LES cloud mask but clear sky in the retrieval cloud mask is only 0.15 % at the finest resolution (Fig R1.1a). For pixels with a very thin optical depth between 0 and 0.05, spatial averaging does increase the mismatch to 4 % around 800 m resolution. However, if only misclassification for retrieved optical depths above 0.1 are considered, the mismatch error does not increase with coarser spatial resolutions.

The mismatch where the LES cloud mask is clear-sky and the retrieval cloud mask is cloudy is slightly larger (Fig R1.1b). This is mainly due to residual noise in the synthetic MONKI simulations. Note that the optical depth of these misclassified pixels is very low. At the finest resolution, the misclassification is below 0.1% in case only misclassified pixels with an optical depth larger than 0.25 are considered. With such small optical depths being retrieved, consequently, GHI errors will remain limited.

3D retrieval

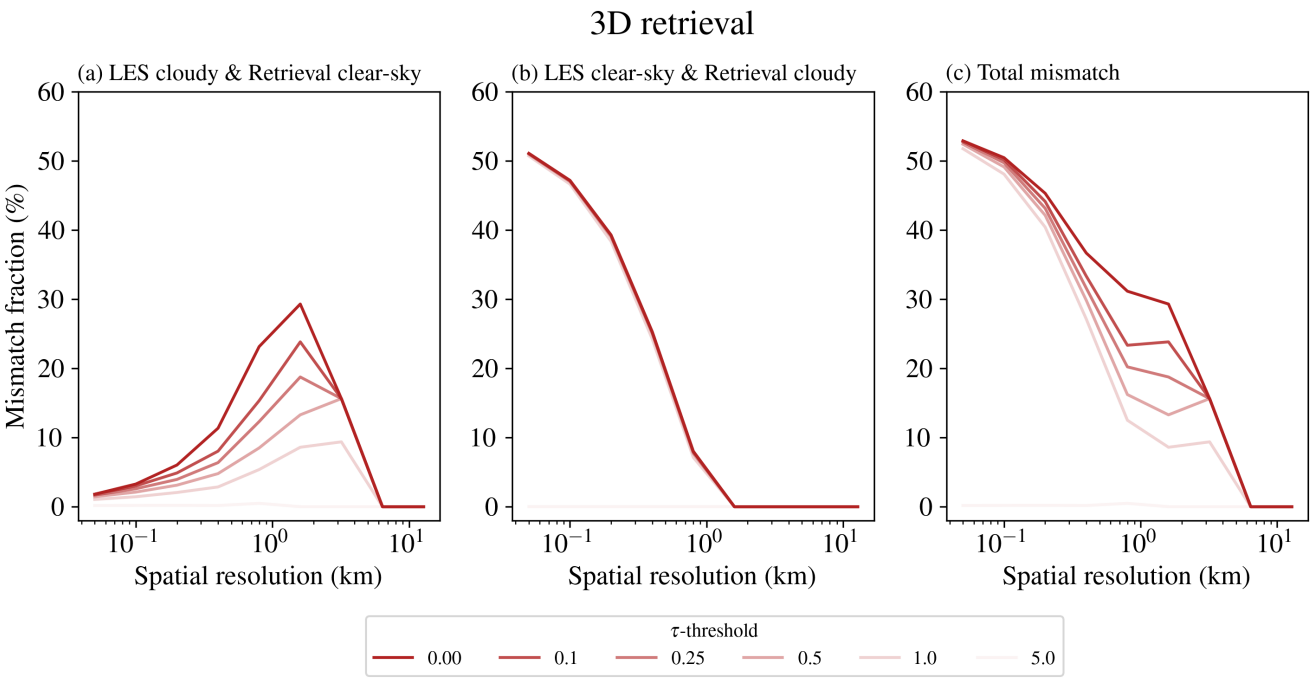

Figure R1.2: Same as Figure R1.1, but now for the 3D retrieval.

In the 3D retrieval, misclassification errors are much more prevalent, which is expected as a result of 3D cloud-radiation interactions. The misclassification of pixels where the LES cloud mask is cloudy and the retrieval cloud mask is clear sky (Fig. R1.2a) is below 2 % at the finest spatial resolution but does increase over 30 % around a 1.6 km spatial resolution. Note that, with spatial averaging, the LES cloud mask becomes increasingly cloudy as more pixels receive an LWP greater than 0. In the retrieval cloud mask, which is based on reflectances, spatial averaging of cloud-shaded pixels with cloudy pixels can cause cloudy pixels to become clear-sky, thus introducing a mismatch.

Finally, we focus on the misclassification for pixels that are clear-sky in the LES cloud mask but cloudy in the retrieval cloud mask (Fig. R1.2b). As it turns out, at the finest spatial resolution, about half of the pixels are misclassified. This can be attributed to errors caused by irradiance enhancement in clear-sky pixels. At coarser resolutions, errors due to irradiance enhancement become less prominent, and the misclassification disappears.

All in all, the misclassification of clear/cloudy pixels in the cloud mask based on reflectance is one of the causes of retrieval errors due to 3D radiative effects. We have decided to exclude the above two figures (R1.1 and R1.2) in the main manuscript. The mechanisms (shading and irradiance enhancements) explaining the trends of figures R1.1 and R1.2 are already described in the manuscript. For instance, in Figure 9 of the manuscript, the relation between reflectance and errors in irradiance enhancement and shading are discussed.

L194: As mentioned in the general comments above, can you include an experiment for intermediate viewing zenith angle (e.g., 35 - 45°) to bridge between overhead (0°) and extreme (70°) view zenith, showing how these compares to the current results. This can be discussed in Section 5.3 L514 to L546.

Initially, we performed the simulation with an extreme viewing zenith angle of 70° to illustrate the possibility of positive clear-cloudy mixing errors. Based on the reviewer's feedback, an additional simulation with a viewing zenith angle of 40° is performed.

The results for VZA=40° will be included in a revised Figure 17. The new scenario will also be added to Table 1. Furthermore, the results will be discussed in Section 5.2, as follows.

Viewing geometry sensitivity

With the relation between clear-cloudy mixing and viewing geometry pointed out in Sect. 5.1, here the scenarios are presented for viewing angles of 40°, and 70°. By evaluating Figure 16 for these two scenarios (also see Table 1), either limited ($\theta = 40°$) or positive ($\theta = 70°$), clear-cloudy mixing biases are expected.

First, for both slanted viewing angles, the PDF of the 1D retrieval is again dominated by high probability densities for the clear-sky pixels (dotted lines, Fig. 17a,d). For the retrieval based on 3D reflectances, clearer deviations are apparent compared to the default scenario. The peak in probability density corresponding to the clear-sky pixels that are incorrectly retrieved as cloudy is closer to the actual clear-sky value than for the default scenario (Compare solid lines of Fig. 17a,d to Fig. 7e). This indicates a smaller error due to irradiance enhancement as the viewing angle increases. Although the peak itself is narrower, in the scenario where $\theta = 70°$, the peak's base is broader than in the default scenario, which we attribute to parallax.

Parallax is the shift between the actual position (from the LES data) and apparent (retrieved) position of an observed object (i.e. clouds). Until this section, all retrievals were performed for nadir viewing angles for which there is no parallax. Slanted viewing results in a shift of the projected location of the clouds in the direction away from the observer. The magnitude of parallax depends on the height of the cloud and the viewing angle. Larger displacements occur for higher clouds or at larger viewing zenith angles. For the retrievals with slanted viewing angles, each pixel will have variable parallax due to variations in cloud occurrence and vertical structure. As a result, clouds that are projected onto a single pixel at nadir viewing might be projected onto multiple pixels at a higher θ, leading to smoother reflectances. If reflectances are smoothed, the retrieved cloud edges become less sharp, resulting in a smoother transition from clear to cloudy in the PDF for retrieved GHI. Due to smoothing, the retrieved cloud fraction effectively increases (not shown). Another effect of the smoothing is that both the fraction of irradiance-enhanced and cloud-shaded pixels is reduced, also reducing the retrieval error due to shading and irradiance enhancement. On the other hand, parallax does introduce an additional mismatch, as clear-sky pixels will be incorrectly classified as cloudy by the retrieval.

At a θ of 40° the change in domain-averaged GHI remains limited (triangular markers in Fig. 17b). Meanwhile, for $\theta = 70°$, an increase in domain-averaged GHI is observed for the 1D retrieval as the resolution gets coarser (triangular markers in Fig. 17e). Both observations are as expected because with a θ of 40°, the clear-cloudy mixing bias remains limited and for $\theta = 70°$, even a positive GHI bias is expected due to clear-cloudy mixing (see Fig. 16).

For the retrievals based on 3D reflectances (cross markers in Fig. 17b,e), towards coarser resolutions, there is an increase in domain-averaged GHI as a result of the increase in relative importance of the retrieval error due to shading over the retrieval error due to irradiance enhancement. However, at coarser spatial resolutions, for both viewing angles, no decrease in domain-averaged GHI is observed as was the case for the default scenario of scene 1. At these coarser resolutions, the influence of irradiance enhancement and shading are limited. Moreover, for these geometries, at coarser resolutions, changes due to clear-cloudy mixing are limited as well (see 1D retrieval 17b,e), and therefore GHI remains unchanged towards even coarser resolutions.

Finally, for the biases (Fig. 17c,f), the IPA-related biases are identical to the default scenario. Since the averaged GHI of the references is constant with resolution, the PPA-related bias follows the same trend as the 1D retrieval. Next, both at a θ of 40° and a θ of 70° a positive trend in residual bias is observed if spatial resolution gets coarser. However, contrary to the scenarios with a nadir view and varying solar zenith angles, albedo, and cloud cover, for the scenario with a θ of 70°, the residual bias remains negative at all spatial resolutions. Overall, for this viewing angle, this results in a negative total bias which vanishes for spatial resolutions of 1.6 km and coarser. Interestingly, at a θ of 40° the total bias is minimal, already at a spatial resolution of 0.2 km. For most other scenarios the total bias reaches its minimum at spatial resolution between 1 and 3 km. What the scenario of $\theta = 40°$ indicates is that the observed minimal biases around 1 km, are not a general rule but heavily depend on the present geometry.

The caption of Figure 17 will be updated to the following.
PDFs of GHI at 0.05 km (a,d) and resolution dependence of domain-averaged GHI (b,e) for the retrieval and reference based on 1D or 3D RT and the biases separated into the contributions due to the PPA, IPA and residual

errors (c,f). The scenario is scene 1 with $\theta = 40°$ (a,b,c), $\theta = 70°$ (d,e,f) and $\phi = 124°$. The solar position is equal to the default scenario with $\theta_0 = 51°$ and $\phi_0 = 184°$.

L525 - 529: "The magnitude of parallax depends on the height of the cloud and the viewing angle." One suggestion is to include a figure of the cloud top height and cloud base height for clouds, this would allow the readers to see the CTH distribution and might envisage how shadowing of one cloud can affect its neighbor, depending on the solar-view geometry.

We have created a figure (see Fig. R1.4, below) illustrating the cloud top height and the degree of parallax displacement for two viewing angles. While it does illustrate the effect of parallax, we are not fully convinced it fits the scope of the current article. In previous work (i.e. Wiltink et al., 2025), we conducted a more in-depth analysis of the effect of parallax on retrieval accuracy, including its relation to cloud top height. Moreover, in Figure 9 of Miller et al. (2018), the relation between zenith angle, cloud top height and parallax is nicely illustrated. Therefore, we have decided not to include this figure in the manuscript; the two references mentioned above will be added after this sentence at l. 525.

P27 l. 525 The magnitude of parallax depends on the height of the cloud and the viewing angle (Miller et al., 2018; Wiltink et al., 2025).

Technical corrections

L7: Abstract indicates resolution range considered as 0.05 to 12.4 km (as well as L80 and L553), while in L207 the largest resolution was stated as 12.2 km. Please standardize (12.2 vs 12.4).
We thank the reviewer for pointing out this inconsistency. In fact, both 12.2 km and 12.4 km are incorrect as the coarsest resolution. The correct value should be 12.8 km. This is because the spatial resolution was doubled in 8 steps from 0.05 to 12.8 km. The values will be been updated throughout the document.

L103: The Solar zenith angle for scene 1 is given as 50.53° but Table 1 and elsewhere often uses 51°. This is okay but clarify rounding.
The value of 50.53° for the solar zenith angle (as well as 184.2° for the solar azimuth angle) is the more precise value used in this study. For clarity, we will round these values to the nearest whole number, which we now also clarify in the text.

Page 4, L103: At 12 UTC the Sun is approximately south [...] a solar zenith angle of 50.53°. In the remainder of the article, these values will be presented rounded to the nearest integer.

L152: Replace "which would additional uncertainties" with "which would cause additional uncertainties"
The text will be modified accordingly.

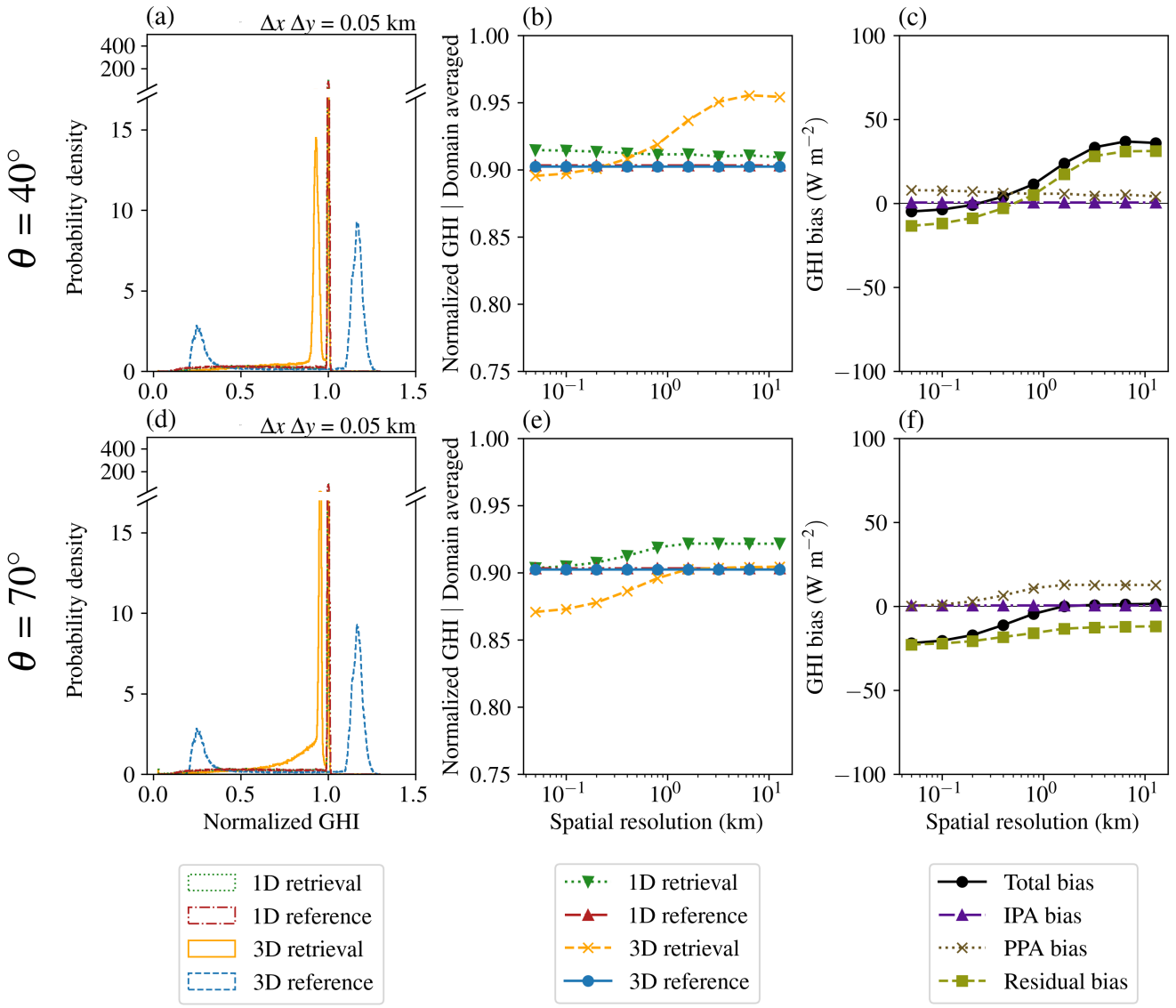

Figure 17: PDFs of GHI at 0.05 km (a,d) and resolution dependence of domain-averaged GHI (b,e) for the retrieval and reference based on 1D or 3D RT and the biases separated into the contributions due to the PPA, IPA and residual errors (c,f). The scenario is scene 1 with $\theta = 40°$ (a,b,c) or $\theta = 70°$ (d,e,f) and $\phi = 124°$. The solar position is equal to the default scenario with $\theta_0 = 51°$ and $\phi_0 = 184°$.

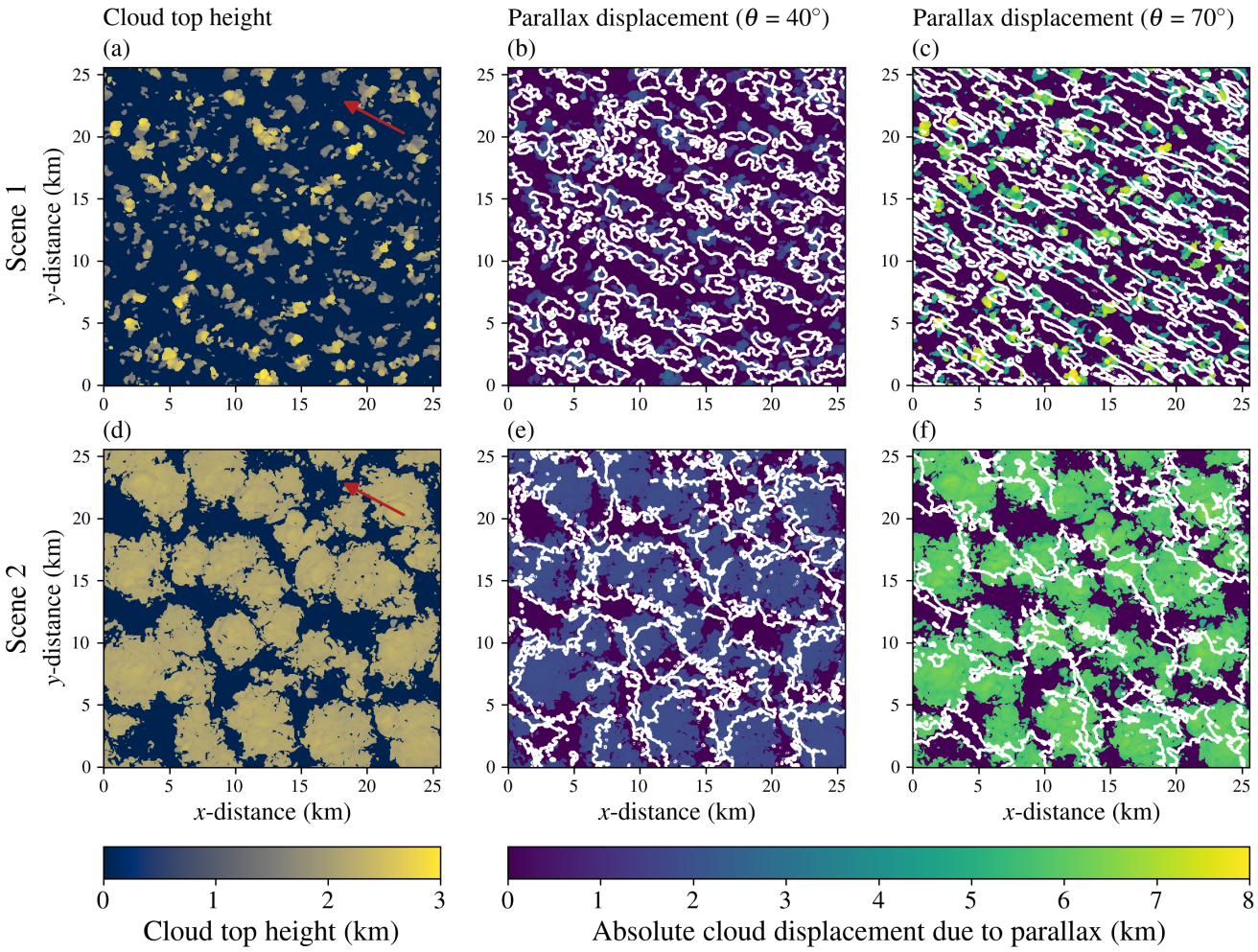

Figure R1.4: Cloud top height of scene 1 (a) and scene 2 (d) along with the absolute cloud displacement due to parallax at viewing angles of 40° and 70° for scene 1 (b,c) and scene 2 (e,f), respectively. The white contours (b,c,e,f) indicate the cloud position uncorrected for parallax. The red arrows in (a,d) indicate the satellite viewing direction.

References

Miller, S. D., Rogers, M. A., Haynes, J. M., Sengupta, M., and Heidinger, A. K.: Short-term solar irradiance forecasting via satellite/model coupling, Solar Energy, 168, 102–117, https://doi.org/10.1016/J.SOLENER.2017.11.049, 2018.

Wiltink, J. I., Deneke, H., van Heerwaarden, C. C., and Meirink, J. F.: Evaluating parallax and shadow correction methods for global horizontal irradiance retrievals from Meteosat SEVIRI, Atmospheric Measurement Techniques, 18, 3917–936, https://doi.org/10.5194/amt-18-3917-2025, 2025.

Reply to report of reviewer #2
"Errors in satellite-based global horizontal irradiance retrievals due to three-dimensional cloud-radiation interactions by Wiltink et. al."

bold italic font = reviewer's comment
regular font = authors' reply
red regular font = original text in the manuscript
blue regular font = newly added or updated text in the manuscript

---

General remarks

This work assesses the uncertainty in satellite-retrieved global horizontal irradiance (GHI) introduced by the independent pixel approximation (IPA) and plane-parallel approximation (PPA) and the corresponding neglect of 3D radiative effects in current retrievals. In particular, the influence of the spatial resolution on the retrieved GHI is analyzed. To this end, a LES cloud field of shallow cumulus clouds is applied. GHI is retrieved from simulated synthetic TOA reflectance and compared to directly simulated GHI for different scenarios (two solar zenith angles, two surface albedos, two cloud fractions) for varying spatial resolutions. The TOA reflectances as well as the simulated reference GHI are computed using both 1D and 3D radiative transfer solvers. Differences between the retrieved and reference GHIs are explained by the relative importance of irradiance enhancements, shading, and clear-cloudy mixing. In addition, the contributions of the IPA and PPA assumptions to the total bias/RMSE is determined and discussed. The findings highlight the importance to account for 3D radiative effects with increasing spatial resolutions of satellite measurements.

The work addresses an important topic, which is very relevant with higher resolution satellite measurements becoming available, and extends previous work on the influence of 3D radiative effects on cloud and radiation retrievals at different spatial resolutions. However, some additional explanations and further discussions as well as language sharpening/improving would be helpful and should be considered before publication. Please see the general and specific comments below.

We thank the reviewer for taking the time to provide a detailed review of our manuscript. Please find our response to the general and specific remarks below.

In general, it would be very helpful to introduce figures properly and define all variables in the text before referencing them. In particular, please add an explanation on how the effective clearsky, irradiance enhancement, and cloud shadow fractions in Fig. 9 and similar figures were determined and better explain the content of the figures before discussing and analyzing it. This makes it much easier for the reader to follow. More detailed comments are provided below.

We have clarified the use of irradiance enhancement, clear-sky, and cloud shadow fraction by introducing the concepts before discussing the figure's content.

L361. ~~To understand [..] (Fig. 9).~~ → To understand this increase in GHI, we need to consider the balance between irradiance enhanced and shaded pixels. To this end, Figure 9 shows the effective clear-sky fraction (round markers), irradiance enhancement fraction (cross markers) and cloud shadow fraction (square markers). The effective clear-sky fraction is derived from the cloud mask based on the LWP from the LES data. Here the term effective indicates that the fraction of pixels with LWP = 0 kg m^{-2} depends on the spatial resolution, whereas the clear-sky fraction

itself does not. The cloud shadow fraction is computed as the fraction of pixels that are clear-sky and located in the shadow of a cloud, where the shadow calculation is based on a geometrical formula using solar position and the cloud top height, following Wiltink et al. (2025). Finally, the irradiance enhancement fraction is defined as the fraction of pixels for which the 0.64 µm reflectance of the 3D retrieval exceeds that of the 1D retrieval by a predefined threshold, here set to 3 ± 1 %.

The caption of Figure 9 now is as follows:
The effective clear-sky fraction, cloud shadow fraction and irradiance enhancement fraction as a function of spatial resolution. The magnitude of the irradiance enhancement fraction is shown for enhancements of 3% (solid line) and 2 to 4 % (shaded area). The scenarios shown are the same as in Fig. 8.

It is stated that cloudy and clear-sky GHI in the retrieval is computed based on a cloud mask using the liquid water path. However, there is a second cloud mask applying the optical thickness. Why are two different cloud masks used? It is not clear to me, why two different cloud masks are necessary and which cloud mask is exactly used for what. Different cloud masks between the different simulated GHIs and retrievals can affect the results and analyses.
Please see our reply to this point in the specific comment below. Similar concerns were raised by reviewer #1. For further details on cloud masking, please see that reply.

I am missing a discussion about other potential error sources, such as e.g. aerosols, the influence of the cloud morphology, and potential limitations of the presented study. In the study, shallow cumulus clouds were considered and differences between two fields of shallow cumulus clouds with different cloud fractions were demonstrated. I would be careful with too general conclusions due to the limited number of configurations with two solar zenith angles, two cloud fractions, and two surface albedos for a nadir viewing geometry and an additional case for a large viewing zenith angle of 70 degree. The importance of 3D radiative effects is influenced by the complex interaction of the solar and viewing geometry, surface albedo, and cloud fraction with mutual influence. In addition, it strongly depends on the cloud type and the related 3D cloud geometry and microphysics.

We agree with both reviewers that we should be cautious about generalising the results of this study to other cloud types or conditions. Therefore, we have decided to include an additional discussion section focusing on generalisability and error sources (see below).

l. 482 To illustrate the implications [...] in Sect 5.2, results are discussed for two final scenarios in which the retrievals are performed with slanted satellite viewing angles. The discussion section ends with an evaluation of the generalisability and remaining error sources of the conducted simulations (Sect. 5.3).

Generalisability and error sources

The current study remains limited to two variable shallow cumulus cloud fields. Results do not necessarily generalise to other cloud conditions. Likely, in more homogeneous scenes, both IPA and PPA errors will be smaller. Future studies should clarify the influence of 3D cloud-radiation interactions on retrieval accuracy in those conditions.

When generalising the presented results, not only cloud conditions should be considered. As we show in the current study, surface albedo and viewing geometry have a considerable influence on the spatial resolution at which the total bias is minimal. While the minimal total bias of the default scenario of scene 1 occurs at a spatial resolution of 1.6 km, this reduces to 0.4 km (surface albedo = 0.0) or even 0.2 km ($\theta = 40°$) in two of the sensitivity experiments.

Furthermore, in terms of RMSE, at resolutions finer than 2 to 6 km, IPA errors are the most important contributor to the overall error. Also, this balance might shift for other cloud conditions or viewing geometries. For instance, in situations with higher cloud cover and a large optical depth variability, relatively larger PPA contributions might be expected.

Although the different error components may vary strongly across cloud conditions and viewing geometries, the mechanisms describing these errors, as explained in this article, remain valid under these varying conditions, albeit

with a different partitioning. Here, we focused on a single retrieval algorithm (i.e., CPP-SICCS), however, similar results would likely have been found using other 1D physics-based retrieval algorithms.

The scenarios presented in this study have been highly idealised, enabling the illustration of the first-order effect of retrieval errors due to spatial inhomogeneity and 3D radiative transfer effects. Compared to non-synthetic satellite retrievals, some deviations are expected.

For instance, for the current simulations, aerosols were excluded. Although the overall radiative effects of aerosols are much smaller than those of clouds, they still influence GHI. In the presence of aerosols, there will be a stronger extinction of irradiance from the direct beam, especially near cloud edges due to aerosol hygroscopic growth, also leading to increased scattering of radiation into cloud shadows (Gristey et al., 2022). For satellite retrievals, increased scattering would result in stronger irradiance enhancement errors in clear-sky regions. On the other hand, increased scattering towards cloud-shaded regions would reduce the errors related to shadowing.

Furthermore, the current study remains limited to a select number of viewing geometries. These results indicate that biases depend on the viewing geometry. Therefore, the methods of the current study should be extended to other geometries to obtain a more general picture of the effect of viewing geometry on retrieval errors arising from three-dimensional cloud-radiation interactions. In terms of PPA, the transmittance biases plotted in Figure 16 already provide a first indication of the sign and magnitude of this error across a range of viewing geometries.

Furthermore, we have nuanced the statement that, **generally**, biases are minimal at a spatial resolution of 1 to 3 km. We decided to do this because for instance, for the scenario with a surface albedo of 0 and a solar zenith angle of 51°, the total bias is minimal at a spatial resolution of 400 m (Fig. 10b). Moreover, for a new simulation with $\theta = 40°$, (see the reply to reviewer #1), the total bias turns out to be minimal at a spatial resolution of 200 m. The following adjustments will be made for this.

Abstract l.6 This study assesses [..] ~~12.4 km.~~ 12.8 km, for varying surface albedos and viewing geometries.
Abstract. l. 11 ~~Generally~~ In most simulations [. . .].

l. 589 ~~Overall, when the separate bias contributions are added up to the total bias, for simulations with surface albedo of 0.22, the smallest total biases are found at a spatial resolution of around 1 to 3 km, which is in line with findings from previous studies.~~ → For most simulations, when the separate bias contributions are added up, the smallest total biases are found at a spatial resolution of around 1 to 3 km, which is in line with findings from previous studies. However, this does not seem to be a general rule as the sensitivity studies show a strong dependence on surface albedo and satellite and solar geometry. For example, at a viewing zenith angle of 40°, total biases are minimal at a spatial resolution of 0.2 km.

Specific comments

l. 38-39: Strictly speaking, the PPA assumes horizontal homogeneity, vertical variations are accounted for.
That is correct: with the PPA, vertical variations are accounted for. Therfore, the sentence will be adjusted to the following:

l. 38-39 The PPA assumes that all retrieved pixels are ~~fully~~ horizontally homogeneous.

l. 41 and 44: These are very general statements. Maybe add references such as Zinner and Mayer (2006).
We have added the reference to Zinner and Mayer after the statement made in l. 41 and 44.

l. 79: Passive imagers can provide information about 3D cloud geometry. In particular, they can resolve horizontal variations and 3D cloud geometry can, for example, also be derived using stereographic methods.
We believe this comment is related to the statement made in l. 71. We agree that it is more precise here to write sub-pixel variability and vertical cloud structure instead of 3D cloud structure. And indeed, with stereographic methods a 3D cloud field could be reconstructed. This would require observations from different platforms with varying viewing geometries, which is beyond the scope of the current study. We have adjusted the statement made

in line 71 to:

Since measurements from individual passive imagers do not give information on ~~3D~~ sub-pixel variability and vertical cloud structure, it remains impossible from these observations alone to quantify exactly how 3D radiative effects and sub-pixel cloud heterogeneity influence GHI retrievals.

l. 95: Could you add at least one or two sentences about the LES simulations giving just a quick summary about the model and data used for the simulations?
We now mention where the full model setup can be found. Furthermore, we now state the radiative transfer solvers (1D and 3D) used by MicroHH. Finally, a reference to the ERA5 Dataset will be added, which is used as input for the MicroHH simulations.

The LES has been performed using MicroHH (Heerwaarden et al., 2017). The full model setup for the current study can be found in Tijhuis (2024). In MicroHH radiation is solved in 1D using RTE-RRTMPG (Radiative Transfer for Energetics+RRTM for General circulations model applications—Parallel; Pincus et al. (2019)) or in 3D using the raytracer of Veerman et al. (2022) (See section 3.3). The initial and boundary conditions are based on ERA5 (Hersbach et al., 2020) [...].

l. 112-118: You state that you excluded gases besides ozone in your radiative transfer simulations, but the satellite retrieval includes the effects of water vapor and CO2. Why did you not include these gases in the simulations as well to avoid inconsistencies? Later in l. 159 you write that the retrieval does not use other gases. Please clarify.
Currently, for MONKI, the effects of other gases besides ozone have not yet been implemented. Therefore, to be consistent, the CPP retrieval of cloud properties was also performed assuming only absorption by ozone. The subsequent SICCS GHI retrieval does include absorption by water vapour and carbon dioxide, in addition to ozone, and is consistent with the reference simulations based on the LES output. This distinction between the cloud property and GHI retrievals is not fully clear in the paper and therefore we will make the following change in l. 159.

l. 165 As mentioned in Sect. 3.1, the MONKI simulations are fully monochromatic, including only absorption by ozone, and the cloud property retrievals are performed correspondingly.

l. 135: How large is the error introduced by using monochromatic simulations instead of directly simulating the satellite channels by performing simulations for a narrow wavelength band and applying the spectral response function of the channels? I guess the retrieval assumes input reflectances for the real satellite channels in contrast to the simulated monochromatic reflectances.
The CPP retrieval is performed assuming monochromatic reflectances, so this is consistent with the MONKI simulations (see previous comment).

l. 160 + 165: You first mention that you flag pixels as cloudy based on the optical thickness. Besides, you have an additional cloud mask using the liquid water path. Why do you use two different cloud masks and when exactly is which cloud mask applied? Differences between the cloud masks and therefore the classification into cloudy and clear sky affect the GHI estimates and therefore the results and analyses.

We primarily use a cloud mask based on the LWP data from LES. However, the CPP-SICCS retrieval uses it's own internal cloud mask based on reflectance. This internal cloud mask for CPP-SICCS is based on reflectance and is therefore more uncertain. As this study shows the reflectance based cloud mask has limitations regarding 3D radiative effects. Furthermore, errors in surface albedo can also cause errors in the reflectance based cloud mask.

The distinction between both cloud masks will be clarified in the manuscript.

l.121 ~~Finally~~ Furthermore, the cloud droplet effective radii of the scene have been rounded to their nearest integer values, in order to align them to the droplet sizes used in MONKI (see Sect. 3.1). Finally, based on LES data a cloud mask is defined by LWP > 0 kg m^{-2}.

The following paragraph has been removed:

l. 165-168 ~~To distinguish between clear-sky and cloudy pixels a cloud mask is generated based on the liquid water path from the LES data. When the liquid water path for a pixel is larger than 0, the pixel is considered to be cloudy. Note that this cloud mask differs from the retrieved optical depths where also for clear-sky pixels a small non-zero optical depth is possible.~~

Finally, in line 161, the difference between both mask is clarified:

Pixels are flagged as cloudy if the retrieved τ is above zero. Note that this internal retrieval cloud mask differs from the LES based cloud mask.

l. 245: Why is the uncertainty of the retrieved optical thickness larger for optically thicker clouds and the optical thickness increasingly overestimated? For optically thick clouds, the reflectance saturates at some point, which would, however, lead to an underestimation of the optical thickness. Please add a short explanation and a reference.
The relation between visible reflectance and optical thickness is indeed non-linear. At higher reflectances, the corresponding optical depth increases rapidly. Therefore, at high optical thickness, a small uncertainty in reflectance will lead to a large uncertainty in optical thickness. (See Fig. 14 of the study of (Platnick et al., 2017))

Regarding the over- or underestimation of retrieved optical thickness we would like to refer to Figure 2 from Nakajima and King (1990) as an illustration. Assume a visible reflectance of 0.7 with an uncertainty of 0.1 then the retrieval will yield:

- Reflectance 0.7 $\rightarrow \tau \approx 32$
- Reflectance 0.6 $\rightarrow \tau \approx 24$ [-8]
- Reflectance 0.8 $\rightarrow \tau \approx 48$ [+16]

The uncertainty in reflectance leads to a mean overestimation of optical thickness.

To clarify this point, the Reference to Platnick 2017 will be added to the manuscript:

This illustrates the increased absolute uncertainty in the τ retrieval for optically thick pixels (Platnick et al., 2017).

l. 250: How did you decide to use a decay scale of 10? The vertical weighting function generally depends on the vertical cloud structure and solar geometry. Did you compute the weighting functions following Platnick (2000)?
We did not compute weighting functions for the specific conditions, but roughly estimated an exponential decay scale from Figure 5a in Platnick (2000). We performed a quick sensitivity study to assess the influence of the vertical weighing on the presented results. For four different values of τ_w, the effective radius retrieval bias for scene 1 and scene 2 is as follows (bias for pixels with $\tau > 3$ between brackets):

- $\tau_w = 1$: 1.61 and 0.50 µm (1.13 and 0.23 µm)
- $\tau_w = 5$: 1.17 and 0.20 µm (0.53 and -0.17 µm)
- $\tau_w = 10$: 1.17 and 0.27 µm (0.53 and -0.09 µm)
- $\tau_w = 15$: 1.20 and 0.31 µm (0.56 and -0.03 µm)

l. 251: Related to the previous point: deviations of the assumed vertical weighting function from the actual one are an additional explanation for the observed differences between the retrieved and the model values.
The vertical weighing is indeed an additional uncertainty in the validation of the effective radii. Since the vertical weighing has only been applied to validate the effective radii simulated with CPP-SICCS against the one from the LES input, it does not play a role in the further analysis presented in the preprint.

l. 306-308: The probability density functions or the average GHIs become much more similar between the different cases at coarser resolutions, but to be honest the spatial distribution to me looks

very different. They all appear kind of noisy but the structures and the absolute values look very different.
Especially for the comparison between the 1D retrieval and 1D reference spatial patterns remain comparable towards lower spatial resolutions. We agree that compared to the spatial patterns of the 3D reference deviations remain larger. We will now formulated the statement differently:

l. 308: Despite the large local differences [..] are smoothed out, and deviations between the 3D and 1D retrievals and reference become less extreme. ~~3D and 1D retrievals and reference converge towards more comparable GHI fields.~~

Fig. 7 and similar figures: This and similar figures are stated to show the probability density function (PDF), but values up to 400 are observed? Are these then absolute frequency values? Please check and clarify.
Yes, these are PDF's, but because the bin sizes of the PDF's are (much) smaller than 1, this allows the probability densities to exceed 1.The total surface area of the PDF still remains 1.

Fig. 8: Could you add the standard deviations to this and similar plots to also visualize the variability?
Adding standard deviations is possible, however, at the finest resolution, the distributions of the 3D reference and retrieval are bimodal. This means that the standard deviation is considerable. For the finest resolution of the default scenario of scene 1 the standard deviation is 0.39 for the 3D reference. Adding standard deviations to these plots, in our opinion, would not lead to further clarification (See added example).

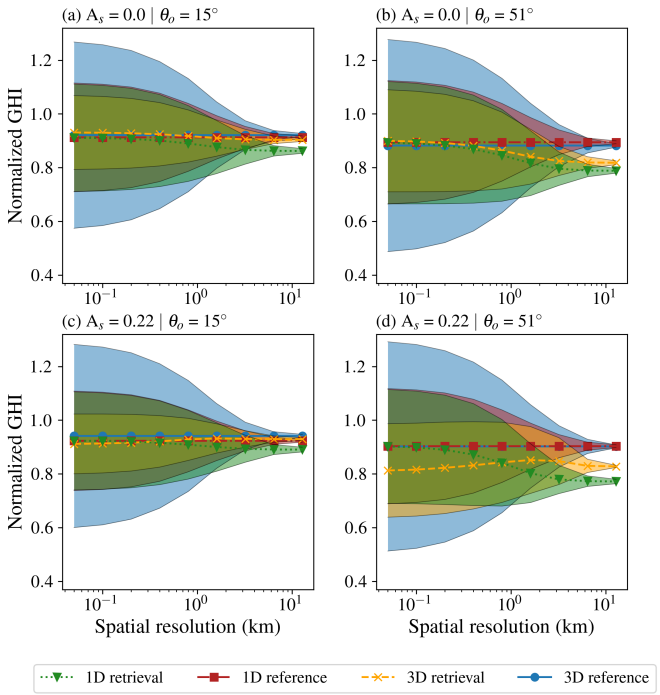

Suggestion 2: Same as Figure 8 in the preprint but now with shaded areas indicating GHI standard deviation

l. 361 / Fig. 9: Please shortly introduce the content of Fig. 9 in the text before using it for the discussion of the results. In particular, please explain how the effective clear-sky fraction, irradiance enhancement fraction and cloud shadow fraction were determined and are defined. These quantities have not been introduced.
See the response to this comment in our reply to the general remarks.

l. 370: Where does the clear-sky reflectance threshold of 0.22 come from?

The explanation presented at l. 370 in the manuscript is based on an older version of the cloud shadow fraction computation, which used reflectance thresholds. The results are very similar to those of the current method, but the presented explanation is not correct.

In our current method, the cloud shadow fraction is defined as the fraction of pixels that are clear-sky and shaded. Whether a pixel is clear-sky or cloudy is determined by the LES cloud mask (and not by reflectance). Shadow pixels are computed using a geometric formula that uses the solar position and cloud-top height. Consequently, the cloud shadow fraction is independent of reflectance. This is will be explained in the beginning of the section (see response to the general remarks of this review) and therefore we will remove the lines 367 – 370.

l. 367 – 371: Meanwhile, it is shown that the cloud shadow fraction (square markers in Fig. 9d) remains constant until a spatial resolution of about 0.8 km ~~The explanation for this is as follows. Cloud shadows are identified as the pixels where the reflectance is below the clear-sky reflectance. Towards coarser spatial resolutions the reflectance of the cloud-shaded pixels gradually increases as mixing with cloudy pixels takes place. But as long as the clear-sky reflectance threshold (in this case 0.22, i.e. the surface albedo) is not exceeded, shadows remain~~, and so does the retrieval error due to shading.

l. 377-385: The solar zenith angle also affects the magnitude of the radiation enhancement not only the number of pixels that are affected. The enhancements are related to radiation escaping through and being reflected on the cloud sides whose orientation relative to the sun matters.

The reviewer correctly points out that the magnitude of the irradiance enhancement is also affected by the solar zenith angle. This information is contained in Figure 9, albeit somewhat indirectly. To get an indication of the magnitude of irradiance enhancements for various scenes, one can consider the ratio between the enhancement fractions.

To illustrate, take the enhancement fractions of 3 and 4 % for the scene with $\theta_0 = 51°$ and a surface albedo of 22 %. About 45 % of pixels have an enhancement larger than 3%, and about 15 % of the pixels have an enhancement above 4 %. This means that 33 % of the pixels with an enhancement above 3% also has an enhancement larger than 4%. A similar comparison can be done for the scene with $\theta_0 = 15°$ and a surface albedo of 22 %. For this scene, the irradiance enhancement fractions are exceeding 3 % and 4 % for about 20 % and 1 % of the pixels, respectively. This means that only 5% of all the pixels with an irradiance enhancement exceeding 3 % also exceed 4 %.

Hence, the distributions of the irradiance enhancement magnitudes differ between the two scenarios. For the high sun scenario, there are relatively much fewer pixels with an enhancement exceeding 4%.

To clarify further, l. 379 will be adjusted to:

l. 379 First, both the irradiance enhancement fraction and magnitude at a θ_0 of 15° is smaller than at a θ_0 of 51° (compare cross markers and shaded areas between Fig. 9c and d). Information on the magnitude of irradiance enhancement can be derived from Fig. 9 by comparing the ratios of irradiance enhancement fractions, for instance, those of 3% and 4%. Relatively, there are much fewer pixels with enhancements exceeding 4% for the high sun scenario than for the low sun scenario. Consequently, at a θ_0 of 15° the corresponding retrieval error is smaller than at a θ_0 of 51° and ~~Hence,~~ the 0.05 km GHI is much closer to the reference.

l. 390: Why are irradiance enhancements absent for a surface albedo of 0? Radiation can still be reflected on the cloud sides or escape through them

We attribute the lack of irradiance enhancements in these scenarios to the absence of albedo enhancement, a mechanism described by Mol and van Heerwaarden (2025). We summarise the effects in lines 326-334 of the preprint. In short, with a surface albedo of 0, every photon that hits the surface is absorbed and does not contribute to irradiance enhancement. The reviewer is correct in pointing out that irradiance enhancements remain possible for photons that do not hit the surface. For the current scenes, this contribution is small but not 0. Since the y-axis of Figure 9 ranges from 0 to 80 %, the small contribution of irradiance enhancement originating from cloud sides is not visible. Therefore, we write that irradiance enhancement is practically absent in scenarios with a surface albedo of 0 %.

Fig. 10/14a: Could you add a horizontal line at 0 to make it easier to distinguish between negative and positive biases

Horizontal lines at y=0 will be added.

Fig. 10 /l. 400-408: In the introduction you stated that the validity of the IPA decreases with increasing spatial resolution. So, I would expect that the error due to the IPA also increases with increasing spatial resolution, but the biases related to the IPA in Fig. 10 appear constant and independent of the resolution.

In this study, the IPA error is defined as the GHI obtained from the 1D reference minus the GHI of the 3D reference. If we average GHI towards coarser spatial resolutions, the domain-averaged GHI remains constant both for the 1D and 3D reference. Hence, the IPA bias remains unchanged. However, the IPA RMSE increases rapidly towards finer spatial scales. Thus, the statement that the IPA validity decreases towards finer spatial resolutions is valid when the RMSE is considered.

l. 411: The error due to the PPA increases towards coarser resolution, in agreement with Zinner and Mayer (2006). Add this reference there.
We will add the reference in the following way:
l. 412 Therefore, the observed PPA [...] mixing in the 1D retrieval. The observation that the error due to PPA increases towards coarser spatial resolutions is in line with previous findings by Zinner and Mayer (2006).

l. 423: The impact of 3D radiative effects might be smaller due to the partial compensation, but it is still not irrelevant. Even for the domain averages large biases remain.
We agree with the reviewer that 3D radiative effects are not irrelevant. Therefore, we will reformulate the statement to the following:

l. 423: ~~Because there is to a large degree a cancellation of the IPA bias due 3D radiative effects such as irradiance enhancement and shading, one might come to the conclusion that 3D radiative effects are irrelevant. While this might be true for the domain averaged bias, locally 3D radiative effects strongly influence the errors as is shown by the RMSE in Fig. 11.~~ → Although the IPA bias turns out to be rather small due to counteracting 3D radiative effects such as irradiance enhancement and shading, 3D radiative effects strongly influence local GHI errors as shown by the RMSE in Fig. 11.

l. 430: Is there a simple explanation, why the residual RMSE is less sensitive to the spatial resolution than the other RMSE components?
Unfortunately, we do not have a simple explanation for this behaviour of the residual RMSE. We decided not to go into detail, as the current reasoning (presented below) remains somewhat speculative.

At fine spatial resolution, the residual RMSE can be strongly influenced by retrieval errors due to irradiance enhancement and shadowing, as manifested in differences between TOA-simulated 3D and 1D reflectances. Towards coarser spatial resolutions these errors gradually disappear. As a result, a decrease in RMSE would be expected. Meanwhile, towards coarser spatial resolution, clear-cloudy mixing errors will increasingly contribute to the RMSE. Clear-cloudy mixing occurs for both 1D and 3D retrievals. However, differences in retrieved τ between 1D and 3D retrievals can lead to clear-cloudy mixing differences that contribute to the residual RMSE. We expect that compensation between these errors will lead to a relatively insensitive residual RMSE as spatial resolution decreases.

l. 470: What do the given percentages refer to? How were they computed?
The reviewer is likely referring to the percentages mentioned in l. 460 and shown, for instance, in Fig. 9. If this is the case, we attempted to clarify this by better introducing Fig. 9 (see the response to the general remarks). In short:

- Effective clear sky fraction: The fraction of clear sky pixels at various spatial resolutions computed using the LWP data of the LES simulation
- Cloud shadow fraction: The fraction of pixels that are clear-sky and shaded. Computed from the cloud top height and the solar geometry following the method of Wiltink et al. (2025).
- Irradiance enhancement fraction: The fraction of pixels where the ratio of the 3D reflectance to the 1D reflectance exceeds a predefined threshold (in Fig. 9 defined between 1.02 and 1.04 (i.e. 2 to 4 % relative difference)).

Fig. 13a: Was the behavior of the PDFs for decreasing resolutions similar to scene 1 in Fig. 7? Yes, despite not being shown in Fig. 13 and Fig. 17, the PDFs gradually converge towards more comparable distributions as the spatial resolution gets coarser.

Sect. 5.1 / Fig. 15: This section was very hard to follow, partly because Fig. 15 and the related methods were not introduced properly. I strongly recommend to rewrite and restructure this section. You could first start with the basic idea: apply the retrieval and average results and compare this to the averaged true values, due to non-linearities you expect differences, and properly explain Fig. 15. To me, it was very unclear at the beginning, what you are explaining and why. The figure caption of Fig. 15 contains new methods and many details which should better be included in the text. Why are geometries close to default used and not the exact default geometries? Please also explain the differences between the different columns and what the dashed lines denote in the figure caption. Section 5.1 is one of the more technical passages of the current preprint. Based on the reviewer's comments above, we have tried to clarify this section.

l. 479: ~~To this end [...] errors due to inhomogeneity.~~ → First, in Sect. 5.1, it is explained in further detail how the averaging of reflectances from adjacent clear and cloudy pixels can introduce errors in the retrieval. Then, to illustrate the [...]

Clear and cloudy sky mixing errors

l. 484-502: To illustrate how clear-cloudy mixing can introduce transmittance biases in the retrieval via reflectance averaging, we assume a new, highly idealised cloud field consisting of just two pixels in this section. The first pixel has a very low optical depth of 0.25, and the other pixel has a τ of either 5, 25 or 90. The satellite and solar geometry of this idealised scenario are taken directly from the DAK LUT (see section 3.2) and closely match the default used in this study (Table 1).

In Figure 15, for the chosen geometry, the relation between reflectance (solid blue curves) and optical depth as well as transmittance (dash dotted green curves) and optical depth are presented for the three optical depth contrasts between $\tau = 0.25$ and $\tau = 5$ (Fig. 15a and d), $\tau = 25$ (Fig. 15b and e) or $\tau = 90$ (Fig. 15c and f), respectively. In Figs. 15a,b,c the narrowband TOA reflectance at 0.64 µm is plotted, while in Figs. 15d,e,f the (hemispheric) broadband TOA albedo is shown.

The relation between τ and reflectance is highly nonlinear, as demonstrated by the solid, blue curves in Figure 15. As a result, coarsening of the the spatial resolution by averaging the retrieved reflectances of the two pixels (indicated by the open blue circles on the reflectance curves), leads to a substantially lower τ than would have been obtained if, instead of reflectances, the optical depth of both pixels would have been averaged (indicated by the crosses on the dashed lines between the reflectance curves).

With the optical depth determined, the next step is to derive surface irradiance. For this, the relation between τ and transmittance is used (indicated by the green dashed-dotted curves). This relation is also highly nonlinear, causing another inhomogeneity error. However, when the narrowband TOA albedo is used to retrieve τ, the relation between transmittance and optical depth is almost exactly the inverse of that between τ and TOA albedo (Figs. 15d,e,f). Hence, if broadband TOA albedo observations are used to retrieve τ and subsequently transmittance, the respective errors cancel out (see also Greuell et al., 2013): the retrieved transmittance for the combined pixel (indicated by the open green circles on the transmittance curves) is very close to the average of the retrieved transmittance for the individual pixels (indicated by the green crosses on the the dotted lines between the transmittance curves).

However, the current study does not use broadband (hemispheric) TOA albedo to derive τ but rather narrowband TOA reflectances, corresponding to measurements from satellite imagers. For these non-hemispheric observations, the relation with τ (solid lines in Figs. 15a,b,c) is slightly different from that for the broadband TOA albedo (solid lines in Figs. 15d,e,f). As a result, depending on the geometry, the τ retrieval offset is not fully compensated for by the transmittance retrieval. Indeed, the retrieved transmittance at coarse resolution (open green circles in Figs. 15a,b,c) is lower than the actual value (green crosses). Notably, if the clear-cloudy contrast grows, the magnitude

of this negative transmittance bias grows accordingly, as indicated by the larger deviation between the horizontal, yellow, dashed lines. [...]

l. 593/594: This is a very general statement. Your study is based on a limited number of configurations for a specific cloud type, namely shallow cumulus clouds. For the analyzed small number of cases, the conclusion is justified, but you should be careful with generalizations. For stratiform clouds, current GHI retrievals might still perform sufficiently well at higher spatial resolutions. In addition, the influence of solar and viewing geometry, surface albedo, cloud fraction, cloud geometry etc. is very complex and cannot easily be separated. You provided a valuable first investigation of different influencing factors, but for a complete picture much more cloud cases and different solar and viewing geometries etc. would have to be analyzed. In addition, aerosol and other factors, which were not accounted for in your study, could also influence the retrieved GHI. Please add a more detailed discussion about this and the limitations of your work.

We agree with the reviewer's comment and have decided to include an additional discussion section. For further details, please see our response under the general comments section.

Technical corrections:

l. 96: add "horizontal" to resolution
The technical correction will be implemented

l. 97: "with a 25 m resolution" → with a resolution of 25m
The technical correction will be implemented.

l. 127: "create synthetic satellite retrievals"→ create synthetic data for satellite retrievals.
The technical correction will be implemented.

l. 152: "which would additional uncertainties" → which would introduce additional uncertainties
The technical correction will be implemented.

l. 172: "which is the mid-latitude summer value" → which is a typical value for the mid-latitudes in summer?
The technical correction will be implemented.

l. 202: assuming independent and homogeneous pixels? 1D means both applying the IPA and PPA.
For the 1D retrieval and reference indeed the IPA and PPA are applied.

l. 207: In abstract and conclusion the coarsest resolution is 12.4 km, whereas here it is 12.2 km.
The correct coarsest spatial resolution actually is 12.8 km. (Also see our reply to reviewer # 1.) This will be corrected in all instances.

l. 238: eliminate the last "resolution".
The technical correction will be implemented.

l. 258: "in 4" → "in Fig. 4".
The technical correction will be implemented.

l. 285: the top 2 rows of Fig 6 show 1D retrieval and 1D reference but you refer to 3D reference and 1D (reference?) GHI fields.
With this sentence the aim is to compare the 1D retrieval against the 3D reference and compare the 1D reference against the 3D reference. To clarify, the sentence will be adjusted.

l.286 At the finest spatial resolutions, there are distinct differences between the 3D reference and the 1D retrieval and reference GHI fields (top 2 rows of Fig. 6).

l. 355: geometry → solar geometry
The technical correction will be implemented.

l. 386: cross and triangular markers?
The statement in l. 386 is indeed true both for the 1D retrieval (triangular markers) and the 3D retrieval (cross markers). The technical correction will be implemented.

l. 502: add: . . . between the horizontal, yellow dashed lines in the middle and right columns.
The technical correction will be implemented.

Fig. 17b: These values are again normalized by clear-sky GHI?
These values have indeed been normalised by the clear-sky GHI.

l. 540: "retrieval 17b" → "retrieval in Fig. 17b"
The technical correction will be implemented.

l. 589: Start a new sentence: . . . total bias. For. . .
The technical correction will be implemented.

In general, I can recommend using Grammarly or similar tools for improving punctuation etc
Grammarly will be used to improve punctuation.

References

Greuell, W., Meirink, J. F., and Wang, P.: Retrieval and validation of global, direct, and diffuse irradiance derived from SEVIRI satellite observations, Journal of Geophysical Research Atmospheres, 118, 2340–2361, https://doi.org/10.1002/jgrd.50194, 2013.

Gristey, J. J., Feingold, G., Schmidt, K. S., and Chen, H.: Influence of Aerosol Embedded in Shallow Cumulus Cloud Fields on the Surface Solar Irradiance, Journal of Geophysical Research: Atmospheres, 127, e2022JD036 822, https://doi.org/10.1029/2022JD036822, 2022.

Heerwaarden, C. C. V., Stratum, B. J. V., Heus, T., Gibbs, J. A., Fedorovich, E., and Mellado, J. P.: MicroHH 1.0: A computational fluid dynamics code for direct numerical simulation and large-eddy simulation of atmospheric boundary layer flows, Geoscientific Model Development, 10, 3145–3165, https://doi.org/10.5194/GMD-10-3145-2017, 2017.

Hersbach, H., Bell, B., Berrisford, P., Hirahara, S., Horányi, A., Muñoz-Sabater, J., Nicolas, J., Peubey, C., Radu, R., Schepers, D., Simmons, A., Soci, C., Abdalla, S., Abellan, X., Balsamo, G., Bechtold, P., Biavati, G., Bidlot, J., Bonavita, M., De Chiara, G., Dahlgren, P., Dee, D., Diamantakis, M., Dragani, R., Flemming, J., Forbes, R., Fuentes, M., Geer, A., Haimberger, L., Healy, S., Hogan, R. J., Hólm, E., Janisková, M., Keeley, S., Laloyaux, P., Lopez, P., Lupu, C., Radnoti, G., de Rosnay, P., Rozum, I., Vamborg, F., Villaume, S., and Thépaut, J.-N.: The ERA5 global reanalysis, Quarterly Journal of the Royal Meteorological Society, 146, 1999–2049, https://doi.org/10.1002/qj.3803, 2020.

Mol, W. and van Heerwaarden, C.: Mechanisms of surface solar irradiance variability under broken clouds, Atmospheric Chemistry and Physics, 25, 4419–4441, https://doi.org/10.5194/ACP-25-4419-2025, 2025.

Nakajima, T. and King, M. D.: Determination of the Optical Thickness and Effective Particle Radius of Clouds from Reflected Solar Radiation Measurements. Part I: Theory, JOURNAL OF THE ATMCBPHERIC SCIENCES, 47, https://doi.org/10.1175/1520-0469(1990)047\%3C1878:DOTOTA\%3E2.0.CO;2, 1990.

Pincus, R., Mlawer, E. J., and Delamere, J. S.: Balancing Accuracy, Efficiency, and Flexibility in Radiation Calculations for Dynamical Models, Journal of Advances in Modeling Earth Systems, 11, 3074–3089, https://doi.org/10.1029/2019MS001621, 2019.

Platnick, S.: Vertical photon transport in cloud remote sensing problems, Journal of Geophysical Research Atmospheres, 105, 22 919–22 935, https://doi.org/10.1029/2000JD900333, 2000.

Platnick, S., Meyer, K. G., King, M. D., Wind, G., Amarasinghe, N., Marchant, B., Arnold, G. T., Zhang, Z., Hubanks, P. A., Holz, R. E., et al.: The MODIS cloud optical and microphysical products: Collection 6 updates and examples from Terra and Aqua, IEEE Transactions on Geoscience and Remote Sensing, 55, 502–525, 2017.

Tijhuis, M.: Code used for publication about coupled 3D radiative transfer, Zenodo [code], https://doi.org/doi.org/10.5281/zenodo.11234716, 2024.

Veerman, M. A., van Stratum, B. J., and van Heerwaarden, C. C.: A Case Study of Cumulus Convection Over Land in Cloud-Resolving Simulations With a Coupled Ray Tracer, Geophysical Research Letters, 49, e2022GL100 808, https://doi.org/10.1029/2022GL100808, 2022.

Wiltink, J. I., Deneke, H., van Heerwaarden, C. C., and Meirink, J. F.: Evaluating parallax and shadow correction methods for global horizontal irradiance retrievals from Meteosat SEVIRI, Atmospheric Measurement Techniques, 18, 3917–936, https://doi.org/10.5194/amt-18-3917-2025, 2025.

Zinner, T. and Mayer, B.: Remote sensing of stratocumulus clouds: Uncertainties and biases due to inhomogeneity, Journal of Geophysical Research: Atmospheres, 111, 14 209, https://doi.org/10.1029/2005JD006955, 2006.